Published in final edited form as:
Magn Reson Imaging. 2013 May ; 31(4): 508–514. doi:10.1016/j.mri.2012.09.003.

Empirical mathematical model for dynamic manganese-enhanced MRI of the murine pancreas for assessment of β-cell function

Anita H. Dhyani, **Xiaobing Fan**, **Lara Leoni**, **Muhammad Haque**, and **Brian B. Roman***
Department of Radiology, University of Chicago, Chicago, IL 60637

Abstract

Autoimmune ablation of pancreatic β-cells and alteration of its microvasculature may be a predictor of Type I diabetes development. A *dynamic* manganese-enhanced MRI (MEMRI) approach and empirical mathematical model was developed to monitor whole pancreatic β-cell function and vasculature modifications in mice. Normal and streptozotocin-induced diabetic FVB/N mice were imaged on a 9.4T MRI system using a 3D magnetization prepared rapid acquisition gradient echo pulse sequence to characterize low dose manganese kinetics in the pancreas head, body and tail. Average signal enhancement in the pancreas (head, body, and tail) as a function of time was fit by a novel empirical mathematical model characterizing contrast uptake/washout rates and yielding parameters describing peak signal, initial slope, and initial area under the curve. Signal enhancement from glucose-induced manganese uptake was fit by a linear function. The results demonstrated that the diabetic pancreatic tail had a significantly lower contrast uptake rate, smaller initial slope/initial area under the curve, and a smaller rate of Mn uptake following glucose activation ($p < 0.05$) compared to the normal pancreatic tail. These observations parallel known patterns of β-cell loss and alteration in supportive vasculature associated with diabetes. Dynamic MEMRI is a promising technique for assessing β-cell functionality and vascular perfusion with potential applications for monitoring diabetes progression and/or therapy.

Keywords

manganese-enhanced MRI; diabetes; rodent pancreas; pancreatic β-cells

1. Introduction

Type 1 diabetes is a chronic pancreatic disease with destruction of insulin producing β-cells at early stages of disease development [1]. To understand the cell loss mechanisms and to monitor therapy, there is a need for early detection. Current trends for early disease detection are based on non-invasive techniques using CT or MRI. MR enables structural and functional imaging that in combination with novel contrast agents [2–4] yields a powerful technique for understanding long-term changes due to disease development. MRI techniques

*Address Correspondence To: Brian B. Roman, Ph.D., Assistant Professor, Department of Radiology, MC2026, University of Chicago, 5841 S. Maryland Ave., Chicago, IL, USA 60637, Phone: (773) 702-6906, broman@uchicago.edu.

have successfully been used to study β-cell mass in vitro and in vivo and most recently to study perfusion by dynamic contrast enhanced (DCE) MRI [5].

Although pancreatic β-cells are located within islets and make up approximately 2% of the pancreatic volume, they receive 20% of the total blood volume [6–8]. In addition to the volume of blood associated with the β-cell, the islet capillaries have been described as being fenestrated and therefore highly permeable compared to neighboring vessels. These unique vascular characteristics suggest an avenue that may be exploited by MRI techniques. Since increased vascular permeability induced by the autoimmune response is believed to be a precursor of disease development [9–14], MRI contrast agents that can enter cells are of great interest for early diabetes detection. A limited number of studies have explored the use of gadolinium (Gd) based contrast agents [15] as well as nanoparticles [16] for detecting vascular changes in diabetic mice. Although these contrast agents are desirable for vascular perfusion studies due to their strong paramagnetic properties and non-toxicity, they remain extravascular and extracellular, providing an indirect link between β-cell viability and vascular contrast enhancement. An alternative and perhaps complementary approach to improve this link is to use a contrast agent that directly correlates with cell activity.

Manganese-enhanced MRI (MEMRI) has been used to measure β-cell function in vitro [17] and in vivo [18–21]. Since manganese (Mn) can enter β-cells via voltage-gated Ca channels [22] and is paramagnetic, thereby providing T_1 contrast in areas of accumulation, this approach provides a direct correlation between β-cell functionality and signal enhancement that enables non-invasive assessment of changes in β-cell mass. In addition, administering an extracellular glucose challenge opens Ca channels and promotes active Mn uptake, reported to double the signal enhancement in comparison to unstimulated or passive Mn uptake [17]. To characterize Mn enhancement in the mouse pancreas, the mathematic model developed by Antkowiak et al. [18] can be applied in cases where signal enhancement plateaus, but may fail to adequately describe contrast kinetics when blood vessels are involved. A model that can account for the presence of vasculature is needed when attempting to describe activation throughout the pancreas, particularly in the pancreatic head where major vessels are present.

In this study, we developed a novel *dynamic* MEMRI technique and empirical mathematical model for monitoring β-cell function in the total pancreatic volume as well as vasculature modifications by linking the functional properties of low dose Mn with the vascular kinetics of dynamic contrast-enhancement. Dynamic MEMRI has potential advantages relative to signal enhancement measurements since real-time cellular and vascular kinetics representative of the ongoing physiological processes can be visualized and quantified. The sensitivity of this technique to β-cell mass and function was demonstrated in the streptozotocin (STZ) mouse model of diabetes [23]. Passive Mn kinetics in regions of interest (ROIs) over the pancreas head, body and tail as a function of time were fit by an empirical mathematical model (EMM) that was expanded from a previous model [24,25]. EMM parameters and kinetic parameters directly calculated from the EMM (initial area under the curve and initial slope of the curve) were used to quantify and/or characterize the various phases of Mn uptake in the pancreas, which may be helpful for developing an analog to link β-cell functionality and vascular alterations to disease development.

2. Methods

2.1. Animal preparation and treatment

A total of 20 (11 normal and 9 diabetic) adult male FVB/N mice of 8–10 weeks in age (Harlan Laboratories, Indianapolis, IN, USA) were used in this study. All procedures were approved by the Institutional Animal Care and Use Committee (IACUC). Animals were

allowed ad libitum access to food and water until 4–6 h prior to imaging, at which time food was withheld. Animals were weighed and their blood glucose measured using a glucometer (Bayer Healthcare, Pittsburgh, PA, USA) prior to imaging.

Diabetes was induced via STZ (Spectrum Chemical Mfg., Gardena, CA, USA) treatment by implementing a single intraperitoneal (IP) injection (188 mg/kg body weight). Animals with serum glucose levels greater than 300 mg/dL prior to imaging were considered diabetic. MR imaging was performed a week after STZ treatment.

Anesthesia was induced using a mixture of 2% isoflurane/98% oxygen via a nose cone. During imaging, respiration, heart rate and body temperature were monitored continuously. Animal temperature was maintained at 37°C by a warm air heating system (SA Instruments, Stony Brook, NY, USA).

2.2. Manganese and glucose

A stock of 1M manganese chloride solution (Sigma-Aldrich, St. Louis, MO, USA) was diluted with isotonic saline solution (Baxter Healthcare, Deerfield, IL, USA) to a working concentration of 20 mM for an average intravenous (IV) bolus infusion of 100 μl (0.08 mmoles/kg). A standard glucose challenge was performed using approximately 100 μl based on BW of a 45% glucose solution (Sigma-Aldrich, St. Louis, MO, USA) for an IP challenge.

2.3. In vivo MRI

MR imaging was performed on a 9.4T Bruker BioSpec scanner equipped with a 12 cm diameter gradient insert BGA12-S (gradient strength of 660 mT/m) (Bruker, Billerica, MA, USA). Animals were placed in a supine position within a Bruker quadrature volume coil (35 mm inner diameter). High-resolution multi-slice coronal FLASH (fast low angle shot) images were acquired first for localization and anatomical visualization of the pancreas (TR/TE = 250/5.2 ms, flip angle = 30°, field of view (FOV) = 50×25 mm, matrix size = 256×128, slice thickness = 0.5 mm, number of excitations (NEX) = 8). Then, on eight slices dynamic Mn-enhanced coronal imaging was performed through the pancreas using a Magnetization Prepared Rapid Acquisition Gradient Echo (MPRAGE) pulse sequence (TR/TE = 9.8/2.9 ms, segment repetition time = 2000 ms, segment duration 627.8 ms, number of segments = 4, flip angle = 10°, FOV = 40×20 mm, matrix size = 128×64, slice thickness = 0.5 mm, inversion time = 700 ms, NEX = 1) with a temporal resolution of ~24 s. An inversion time was selected so that the pancreatic signal was nulled prior to the administration of Mn. Six pre-contrast images were acquired, after which a slow IV Mn bolus was delivered over 1 min using a syringe infusion pump (Harvard Apparatus, Holliston, MA, USA) to a total dose of 10 μg/kg body weight. The same pulse sequence was repeated over the remaining ~28 minutes during Mn uptake and accumulation. An IP glucose bolus (1.5 g/kg body weight) was administered at ~30 min of the dynamic series and dynamic image acquisition continued for 20 min. Total imaging time including animal setup was less than 90 min.

2.4. MRI data analysis

Image reconstruction, processing and analysis code was written in MATLAB 7.70 R2008b (Mathworks, Natick, MA, USA). ROIs were drawn on anatomical images and superimposed on dynamic images. ROIs consisted of contiguous regions of the left and right kidneys and the head, body, and tail of the pancreas as was visible in the imaged slices. The head, body, and tail of the pancreas were approximately 3 mm each. The tail was defined to be adjacent to the spleen, the body was defined to be inferior to the stomach, and the head was the furthest extent of the pancreas adjacent to the stomach.

The average signal intensity (S(t)) of the dynamic MRI series over a selected ROI for each slice was calculated as a function of time. A previous study demonstrated that the normal mouse kidney Mn enhancement reaches a plateau at ~10 min post-Mn injection [20] and the signal intensity changes in the pancreas and the kidney were proportional to injected dose. Due to animal weight dependent coil loading variance, S(t) was normalized by the average signal enhancement of the kidney at 30 min to facilitate inter-experiment comparison using the following equation:

$$\Delta S(t)=(S(t)-S_0)/S_{kidney} \quad (1)$$

where S_0 is the averaged signal in pre-contrast images and S_{kidney} is the averaged signal enhancement at 30 min in the kidney. In order to quantitatively analyze the Mn enhancement in the ROIs, we developed a new model with the robustness to fit kinetic data that are indicative of vasculature that may not be visually apparent. ΔS(t) was fitted by the following EMM to characterize Mn uptake and washout:

$$\Delta S(t)=A\cdot(1-e^{-\alpha t})\cdot e^{-\beta t}\cdot(1+\varepsilon e^{-\gamma t}) \quad (2)$$

where $A(1+\varepsilon)$ is the upper limit of the signal intensity and α (min^{-1}) is the rate of contrast uptake. Washout is modeled as a bi-exponential process with a slow component (β (min^{-1})) and a more rapid component (γ (min^{-1})) that accounts for contrast kinetics without and with vasculature present in the ROI, respectively. With proper combination values ε and γ, the term ($1+\varepsilon e^{-\gamma t}$) modulates the original EMM to more accurately express contrast kinetics in regions of the pancreas that contain blood vessels. When the blood vessel effect was not dominant, ε approached zero and Eq. (2) reduced to a simple EMM model [25].

In addition, the following commonly used parameters were directly calculated from the EMM parameters to mitigate the effects of noisy data:

a. **Initial area under the curve iAUC$_\tau$**: The iAUC$_\tau$ was calculated by integrating over Eq. (2), i.e.,

$$\mathrm{iAUC}_\tau=A\cdot\left[\frac{1-e^{-\beta\tau}}{\beta}+\frac{e^{-(\alpha+\beta)\tau}-1}{\alpha+\beta}\right]+A\cdot\varepsilon\cdot\left[\frac{1-e^{-(\alpha+\beta+\gamma)\tau}-1}{\alpha+\beta+\gamma}\right] \quad (3)$$

where τ is the time over which the signal was integrated, which was equal to 2 min in this study.

b. **Initial slope of the curve (iSlope):** The iSlope was obtained by taking the derivative of Eq. (2) for $t \ll 1$, yielding:

$$\mathrm{iSlope}\approx A\cdot\alpha\cdot(1+\varepsilon) \quad (4)$$

Finally, glucose stimulation of β–cells and its affect on Mn kinetics was modeled by fitting the following linear equation to $\Delta S(t)$:

$$\Delta S(t)=m_g\cdot t+b \quad (5)$$

where m_g is the slope and b is the intercept. The slope of the passive Mn curve (m_m) just prior to glucose administration was calculated from the EMM-fitted $\Delta S(t)$ at 20 and 30 min. Then, the change in Mn kinetics from passive to active uptake was quantified by calculating the angle between two lines, governed by the slopes m_m and m_g as follows:

$$\cos\theta = \frac{1 + m_m m_g}{\sqrt{1 + m_g^2} + \sqrt{1 + m_m^2}} \quad (6)$$

where the angle θ was in degrees.

2.5. Statistical analysis

Statistical analysis was performed using Matlab. Model parameters for each slice within an animal were averaged and compared between normal and diabetic mice. Differences between mean model parameters for normal and diabetic mice were evaluated using the Wilcoxon Ranksum test, where $p < 0.05$ indicated statistical significance. Values are shown as mean ± SD.

3. Results

ROI analysis for assessment of signal enhancement in the pancreas and/or kidney was performed on a total of 11 normal (fasting blood glucose 166±18 mg/dl) and 9 STZ-induced diabetic mice (fasting blood glucose 405±111 mg/dl). Figure 1 shows representative anatomical images of the right kidney (left panel) and associated plots of ΔS(t) (right panel) for a normal (top) and diabetic (bottom) mouse. Overall averaged ROI areas in the right kidney and left kidney were 30±9.4 mm^2 and 37±10 mm2, respectively. ΔS(t) for the normal (open circle) and diabetic (open triangle) mouse were fitted by the original EMM (black dashed line) for passive uptake and the linear function (gray solid line) for active uptake. The EMM accurately fit the passive uptake regions, while the linear function accurately fit the activation regions for both normal and diabetic mice. Both normal and diabetic kinetic curves reached a plateau by 30 min and were unaffected by glucose administration. A summary of averaged normalized EMM parameters (α, β, A) and angle (θ) are given in Table 1 for both normal and diabetic mouse kidney. No significant differences were seen between model parameters from the EMM fit ($p > 0.2$) as well as from the linear fit ($p = 0.07$), indicating similar responses in the normal and diabetic kidney to contrast administration. In addition, the absolute kidney Mn enhancement at 30 min (average of left and right kidneys) was similar between normal (1.6±0.3) and diabetic (1.5±0.4) mice.

Due to the physiological motion as well as the non-uniform distribution of the pancreas, it was not possible to delineate a pancreatic ROI in each of the eight slices obtained from the image volume. Overall averaged ROI areas in the tail, body, and head were 4.3±0.1 mm^2, 4.8±2.0 mm^2, and 6.7±2.4 mm^2, respectively. The number of mice with pancreatic ROIs and the average number of slices for each ROI are summarized in Table 2. The pancreatic tail was identified in all animals and in the largest number of slices, whereas the pancreatic head was the most difficult to identify and therefore was represented by the smallest number of slices. Figure 2 shows a typical example of passive and active uptake for a normal (top) and diabetic (bottom) mouse with the anatomic MRI of the pancreas tail (left panel) and the associated plots of $\Delta S(t)$ (right panel). Again, the EMM and linear function accurately fit passive and active regions. Figure 2 illustrates that passive Mn uptake is more rapid in the normal pancreatic tail in comparison to the diabetic pancreatic tail (1.44 min vs. 1.32 min^{-1}). In addition, this figure shows that glucose-induced β-cell activation resulted in a greater Mn washout in comparison to the diabetic mouse (0.50° vs. 0.28°). A summary of the averaged EMM parameters (α, β, A) and angles (θ) for all of the normal and diabetic mice pancreata studied are given in Table 3. Passive Mn uptake was significantly slower in the diabetic pancreatic tail in comparison to the normal pancreatic tail ($p < 0.05$). Glucose

activation of β-cells resulted in a significantly greater response in the normal pancreatic tail, indicated by larger values for θ, in comparison to diabetic animals ($p < 0.05$).

Analyses were performed across the length of the pancreas in order to determine possible differences in regional uptake. The kinetic curves generated from overall averaged EMM parameters are illustrated in Fig. 3. Qualitative assessment of the curves indicates regional differences with the head being differentiated in the initial phase and the body and tail in the amplitude and later phase of washout. The normal pancreatic tail (top), body (middle), and head (bottom) had a more rapid contrast uptake and slower washout than diabetic counterparts. However, statistical significance was not reached in the pancreatic body and head for averaged EMM parameters between normal and diabetic mice. The kinetics from the pancreatic head is unique compared to other areas, in which an early rapid uptake region followed by rapid washout in the form of a distinct peak was observed. This region is followed by a later phase of uptake or washout. In contrast, both the pancreatic tail and body in the top and middle panels demonstrate an uptake period that transitions into the washout period without a distinct peak. The complex shape of the pancreatic head signal enhancement curve suggestive of vasculature could not be accurately fit by the EMM. The introduction of ε was required for a best fit in greater than 70% of the normal and diabetic pancreatic head ROIs. In the remaining 30% of the pancreas, ε approaches zero indicating ROIs lacking major vasculature. Finally, the parameters iSlope and iAUC are plotted in Fig. 4. The iSlope and iAUC in the tail decreased following the development of diabetes, although no significant differences were observed in the other regions of the pancreas. The impact of β-cell content on the contrast kinetics seen in Fig. 3 and Table 3 also influences the iSlope and iAUC.

4. Discussion

As a complementary approach to the development of PEGylated gadolinium DCE-MRI by Medarova and Moore [15], our study assesses β-cell function throughout the entire pancreas in vivo by the development and application of *dynamic* MEMRI. Using Mn as a T_1 contrast agent actively regulated through L-type Ca channels [22], we examined its ability to be used as a dynamic contrast agent for probing β-cell viability and pancreatic perfusion associated with diabetes [17–19,21,26]. The kinetic models developed here were able to describe the uptake and washout of Mn before and following glucose stimulation in three distinct regions of the pancreas. These kinetic analyses demonstrate that, particularly in the tail region of the pancreas, Mn uptake and response to glucose was diminished due to diabetes. However, it appeared that the introduction of glucose in this study resulted in decreased Mn contrast and apparent Mn washout, which would seem to contradict this and our previous studies [17,22,27]. Although in vivo intracellular Mn uptake and metabolic pathway in β-cells have not been specifically identified, it can be hypothesized that the decrease in contrast seen after glucose delivery be due to multiple phenomena. As our in-vitro studies suggest, following intracellular increase in Mn concentration due to glucose stimulation, the ions could be sequestered in the secretory pathway and loose their access to water. However, there are differences between in vitro and in vivo experiments, and more works on this phenomena are needed to elucidate the in vivo mechanism.

Differences in pancreatic perfusion between normal and diabetic animals have been confirmed by several studies that have shown pancreatic vascular alterations are a precursor to diabetes development [9–14]. One of the major challenges for pancreatic MRI is obtaining a complete image covering the pancreas from head to tail. This is particularly problematic in the mouse as the pancreas is 2 – 3 mm thick and 2–3 cm long with a relatively low tissue density. Therefore obtaining a sufficient number of ROIs per slice is difficult. The tail region is most often described in imaging studies due to the clear

anatomical landmarks and minimal motion. These complications are exacerbated, notably by respiratory motion that is more prevalent in the head. As β-cells are widely distributed in the pancreas, it is important to completely image the pancreas.

The head of the pancreas had the greatest variance (Table 2) that was due to fewer animals with clear head boundaries along with fewer ROIs per slice, both of which could be improved by decreasing slice thickness and increasing signal averaging. Acquiring anatomic MR images of the pancreatic tail (Fig. 2) provided confirmation that the data was obtained from the tail; this ROI also represents a significant volume (4.3 mm^3) per slice. With 3–8 slices per pancreas, the measured tail volume was approximately 19.0 mm^3 or approximately 50% of the total pancreatic volume with the body and head comprising 10 and 5 mm^3 respectively. This is far greater than other in vivo studies [18,19] and therefore a more representative assessment of the total β-cell population. Kinetic plots $\Delta S(t)$ illustrate that non-glucose activated Mn uptake is less rapid in the diabetic pancreatic tail in comparison to the normal pancreatic tail (1.32 min^{-1} vs. 1.44 min^{-1}). The lower uptake is likely due to a decrease in vascular function and the number of β-cells associated with diabetes. During the development of diabetes, the pancreas undergoes an inflammatory response similar to changes associated with pancreatitis and results in decreased perfusion due to a combination of microcirculatory and compliance/elasticity changes in the parenchyma [28].

Figure 2 and Table 2 show that glucose-induced β-cell activation resulted in greater Mn washout rate in comparison to the diabetic mouse (0.50° vs. 0.28°). Although the increase in enhancement during the passive phase can be attributed to differences in beta cell population and vascular structure, changes following activation are likely due to vascular changes due to the time between Mn infusion and glucose administration. Figure 3 shows the head of the pancreas demonstrates a very rapid uptake followed by a similarly rapid washout. This pattern is not characteristic of tissue but indicative of blood vessels. The vascular changes resulting in diminished perfusion in cases of pancreatitis are most dramatic in the head of the pancreas [29] and would explain the diabetic kinetics. This potential sensitivity to the presence of vessels warrants further experimental investigation but could be quite powerful in monitoring the progression of the disease and therapeutic effectiveness. Following glucose stimulation the resulting increase in blood flow supports the Mn washout seen in the normal pancreas with a change in θ. The absence of this response in the diabetic pancreas may be attributed to an increase in interstitial pressure and decreased blood flow [13]. The summary of kinetic curves in Fig. 4 clearly illustrate the regional differences in signal enhancement across the pancreas with the most striking regional difference found in the head of the pancreas.

An extension of the kinetic modeling was developed resulting in a new form of the EMM that accounted for contrast kinetics both with and without the presence of a vessel. This can be attributed to the presence of four vessels originating from the bifurcation of the superior and inferior pancreaticoduodenal arteries [30]. However, both the tail and body of the pancreas demonstrated slower washout since these regions are supplied by ten smaller arteries, and so were appropriately modeled by the reduced form of Eq. [2]. Most studies performing DCE-MRI of the pancreas draw the largest possible ROIs that exclude surrounding vessels [31,32] due to the complex modeling necessary to accurately describe the kinetics. Since vascular perfusion is widely assessed using Gd based chelates [15,33], we performed T1-weighted dynamic Gd-DTPA enhanced MRI in the pancreas of normal and diabetic mice to ascertain the bulk flow kinetics. However, the thick slices (> 1 mm) and the required high temporal resolution to detect dynamic contrast uptake made it difficult to obtain images with adequate signal for delineating the pancreas (Data not shown).

Although our study demonstrated significant kinetic differences between the normal and diabetic pancreatic tail, there are two limitations. First, motion artifacts in an MR image makes identifying the pancreas difficult and curve fitting to be less accurate. Since the tail is attached to the spleen and bounded by the stomach and kidney, it was the least prone to motion artifacts in comparison to the body or head, enabling identification of a greater number of ROIs and resulting in the clear statistical trends. Fasting the animals for 4–6 h prior to imaging helped to reduce motion artifacts [34] but not eliminate them. Second, conducting a dynamic perfusion study in the abdominal region requires the use of a pulse sequence with a high temporal resolution that can adequately capture contrast kinetics, decrease non-specific abdominal contrast and is sensitive to the thin pancreas. The tradeoff is that the signal-to-noise ratio present is often too low to delineate anatomical structures. The feasibility of using these perfusion parameters to make a diagnosis of early diabetes remains to be demonstrated. Here we were able to visualize the structures using a modest temporal resolution; however, further investigations into pulse sequences that can provide a higher temporal resolution with adequate pancreatic signal is needed, since less noise would reduce inter-data set standard deviations.

5. Conclusions

In conclusion, dynamic MEMRI can provide unique access to the dynamic functional changes associated with diabetes as it links both organ perfusion and cell function. Kinetic parameters derived from the EMM differentiated the normal from diabetic pancreatic tail. In addition, the change in image contrast as induced by glucose was greater in the normal than in the diabetic pancreatic tail. Compared to simple measurements of enhancement, the detailed kinetic modeling performed here provided parameters that could be used as biomarkers for disease detection. Our bolus infusion low-dosage administration of Mn is a valuable technique that has the potential to translate to the clinical setting as a non-invasive tool to follow diabetes progression and response to therapy in the future.

Acknowledgments

This work was supported by grants from the Cancer Research Foundation, the National Institute of Biomedical Imaging and Bioengineering (RO1 EB003108-01), and the Beta Cell Biology Consortium. We would like to thank Dr. Gregory Karczmar for reviewing the manuscript and Marta Zamora, Erica Markiewicz, and Jim Vosicky for performing the animal set-up.

References

1. Sedimbi SK, Sanjeevi CB. Prevention of beta-cell destruction in autoimmune diabetes: current approaches and future prospects. Adv Exp Med Biol. 2010; 654:611–626. [PubMed: 20217516]
2. Atri M. New technologies and directed agents for applications of cancer imaging. J Clin Oncol. 2006; 24:3299–3308. [PubMed: 16829654]
3. Luo K, Liu G, He B, Wu Y, Gong Q, Song B, et al. Multifunctional gadolinium-based dendritic macromolecules as liver targeting imaging probes. Biomaterials. 2011; 32:2575–2585. [PubMed: 21256587]
4. Oghabian MA, Farahbakhsh NM. Potential use of nanoparticle based contrast agents in MRI: a molecular imaging perspective. J Biomed Nanotechnol. 2010; 6:203–213. [PubMed: 21179937]
5. Naish JH, Hutchinson CE, Caunce A, Roberts C, Waterton JC, Hockings PD, et al. Multiple-bolus dynamic contrast-enhanced MRI in the pancreas during a glucose challenge. J Magn Reson Imaging. 2010; 32:622–628. [PubMed: 20815060]
6. Lifson N, Kramlinger KG, Mayrand RR, Lender EJ. Blood flow to the rabbit pancreas with special reference to the islets of Langerhans. Gastroenterology. 1980; 79:466–473. [PubMed: 7000613]
7. Lifson N, Lassa CV, Dixit PK. Relation between blood flow and morphology in islet organ of rat pancreas. Am J Physiol. 1985; 249:E43–48. [PubMed: 2409813]

8. Jansson L, Hellerstrom C. A rapid method of visualizing the pancreatic islets for studies of islet capillary blood flow using non-radioactive microspheres. Acta Physiol Scand. 1981; 113:371–374. [PubMed: 7048853]
9. Bonner-Weir S, Orci L. New perspectives on the microvasculature of the islets of Langerhans in the rat. Diabetes. 1982; 31:883–889. [PubMed: 6759221]
10. Chakir M, Plante GE. Endothelial dysfunction in diabetes mellitus. Prostaglandins Leukot Essent Fatty Acids. 1996; 54:45–51. [PubMed: 8992493]
11. De Paepe ME, Corriveau M, Tannous WN, Seemayer TA, Colle E. Increased vascular permeability in pancreas of diabetic rats: detection with high resolution protein A-gold cytochemistry. Diabetologia. 1992; 35:1118–1124. [PubMed: 1478363]
12. Henderson JR, Moss MC. A morphometric study of the endocrine and exocrine capillaries of the pancreas. Q J Exp Physiol. 1985; 70:347–356. [PubMed: 3898188]
13. Papaccio G. Insulitis and islet microvasculature in type 1 diabetes. Histol Histopathol. 1993; 8:751–759. [PubMed: 8305825]
14. Yamamoto M, Nakajo S, Tahara E, Ito M, Taniyama K, Shimamoto F, et al. Mucosal changes of the gallbladder in anomalous union with the pancreatico-biliary duct system. Pathol Res Pract. 1991; 187:241–246. [PubMed: 2068006]
15. Medarova Z, Castillo G, Dai G, Bolotin E, Bogdanov A, Moore A. Noninvasive magnetic resonance imaging of microvascular changes in type 1 diabetes. Diabetes. 2007; 56:2677–2682. [PubMed: 17682091]
16. Turvey SE, Swart E, Denis MC, Mahmood U, Benoist C, Weissleder R, et al. Noninvasive imaging of pancreatic inflammation and its reversal in type 1 diabetes. J Clin Invest. 2005; 115:2454–2461. [PubMed: 16110329]
17. Gimi B, Leoni L, Oberholzer J, Braun M, Avila J, Wang Y, et al. Functional MR microimaging of pancreatic beta-cell activation. Cell Transplant. 2006; 15:195–203. [PubMed: 16719054]
18. Antkowiak PF, Tersey SA, Carter JD, Vandsburger MH, Nadler JL, Epstein FH, et al. Noninvasive assessment of pancreatic beta-cell function in vivo with manganese-enhanced magnetic resonance imaging. Am J Physiol Endocrinol Metab. 2009; 296:E573–578. [PubMed: 19116376]
19. Patel AR, Antkowiak PF, Nandalur KR, West AM, Salerno M, Arora V, et al. Assessment of advanced coronary artery disease: advantages of quantitative cardiac magnetic resonance perfusion analysis. J Am Coll Cardiol. 2010; 56:561–569. [PubMed: 20688211]
20. Lee LW, So PW, Price AN, Parkinson JR, Larkman DJ, Halliday J, et al. Manganese enhancement in non-CNS organs. NMR Biomed. 2010; 23:931–938. [PubMed: 20878971]
21. Lamprianou S, Immonen R, Nabuurs C, Gjinovci A, Vinet L, Montet XC, et al. High-resolution magnetic resonance imaging quantitatively detects individual pancreatic islets. Diabetes. 2011; 60:2853–2860. [PubMed: 21926272]
22. Leoni L, Serai SD, Haque ME, Magin RL, Roman BB. Functional MRI characterization of isolated human islet activation. NMR Biomed. 2010; 23:1158–1165. [PubMed: 21162143]
23. Arora S, Ojha SK, Vohora D. Characterisation of streptozotocin induced diabetes mellitus in swiss albino mice. Global Journal of Pharmacology. 2009; 3:81–84.
24. Fan X, Medved M, Karczmar GS, Yang C, Foxley S, Arkani S, et al. Diagnosis of suspicious breast lesions using an empirical mathematical model for dynamic contrast-enhanced MRI. Magn Reson Imaging. 2007; 25:593–603. [PubMed: 17540270]
25. Jansen SA, Fan X, Karczmar GS, Abe H, Schmidt RA, Newstead GM. Differentiation between benign and malignant breast lesions detected by bilateral dynamic contrast-enhanced MRI: a sensitivity and specificity study. Magn Reson Med. 2008; 59:747–754. [PubMed: 18383287]
26. Leoni L, Roman BB. MR imaging of pancreatic islets: tracking isolation, transplantation and function. Curr Pharm Des. 2010; 16:1582–1594. [PubMed: 20146663]
27. Leoni L, Dhyani A, La Riviere P, Vogt S, Lai B, Roman BB. beta-Cell subcellular localization of glucose-stimulated Mn uptake by X-ray fluorescence microscopy: implications for pancreatic MRI. Contrast Media Mol Imaging. 2011; 6:474–481. [PubMed: 22144025]
28. Reber HA, Karanjia ND, Alvarez C, Widdison AL, Leung FW, Ashley SW, et al. Pancreatic blood flow in cats with chronic pancreatitis. Gastroenterology. 1992; 103:652–659. [PubMed: 1634080]

29. Delrue L, Blanckaert P, Mertens D, Van Meerbeeck S, Ceelen W, Duyck P. Tissue perfusion in pathologies of the pancreas: assessment using 128-slice computed tomography. Abdom Imaging. 2011

30. Andersen, DK.; Brunicardi, C. Chapter: Pancreatic Anatomy and Physiology. In: Greenfield, LJ.; Mulholland, MW.; Oldham, KT.; Zelenock, GB.; Lillemoe, KD., editors. Essentials of surgery: scientific principles and practice. Lippincott Williams & Wilkins; 1997. p. 235.241

31. Bali MA, Metens T, Denolin V, De Maertelaer V, Deviere J, Matos C. Pancreatic perfusion: noninvasive quantitative assessment with dynamic contrast-enhanced MR imaging without and with secretin stimulation in healthy volunteers--initial results. Radiology. 2008; 247:115–121. [PubMed: 18292476]

32. Ichikawa T, Haradome H, Hachiya J, Nitatori T, Araki T. Perfusion-weighted MR imaging in the upper abdomen: preliminary clinical experience in 61 patients. AJR Am J Roentgenol. 1997; 169:1061–1066. [PubMed: 9308465]

33. Leach MO. Application of magnetic resonance imaging to angiogenesis in breast cancer. Breast Cancer Res. 2001; 3:22–27. [PubMed: 11300102]

34. Grimm J, Potthast A, Wunder A, Moore A. Magnetic resonance imaging of the pancreas and pancreatic tumors in a mouse orthotopic model of human cancer. Int J Cancer. 2003; 106:806–811. [PubMed: 12866043]

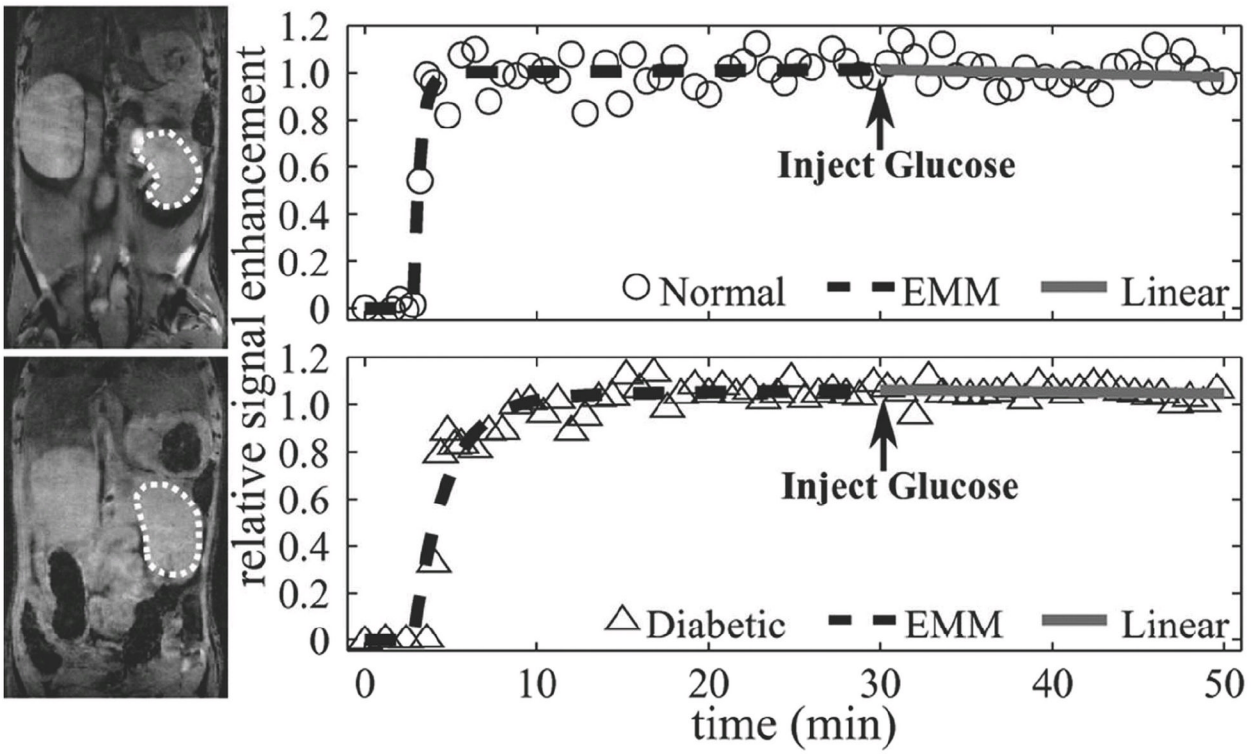

Figure 1.

Renal MR images and their corresponding uptake curves. The region of interest is outlined by a dashed line. Signal enhancement data (circle = normal, triangle = diabetic) for passive and active regions of Mn uptake were fit by an EMM (dashed line) and a linear function (solid line), respectively. Signal enhancement reached a plateau for both normal and diabetic kidneys by 30 min. Glucose-induced activation did not change the trajectory of the washout region ($p > 0.05$) in normal and diabetic animals.

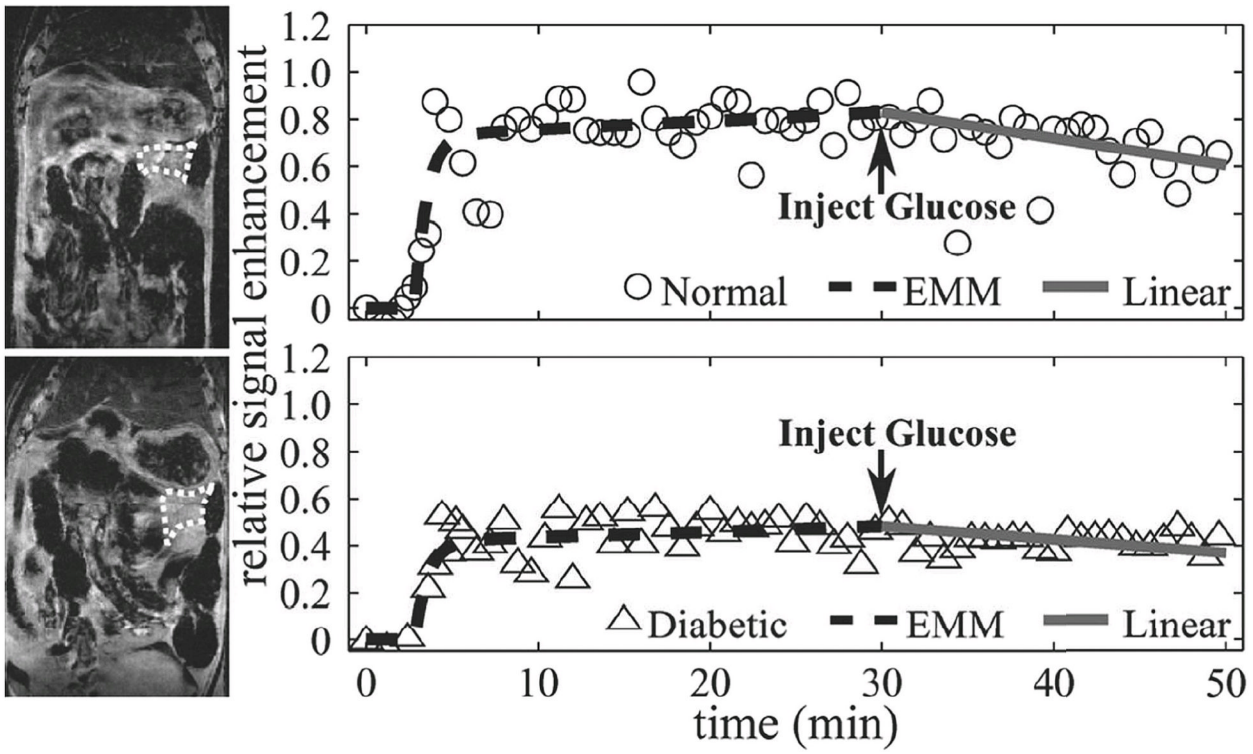

Figure 2.

Representative anatomical pancreatic tail MR images and corresponding kinetic curves for a normal (top panel) and a diabetic (bottom panel) mouse. The region of interest is outlined by a dashed line. Signal enhancement data (circle = normal, triangle = diabetic) for passive and active regions of Mn uptake were fit by an EMM (dashed line) and a linear function (solid line), respectively. The uptake rate was significantly lower for diabetic animals ($p < 0.05$), but no differences were found in the peak signal and washout rate between normal and diabetic mice. Glucose-induced activation in normal animals resulted in significantly larger angles between passive and active uptake curves in comparison to diabetic animals.

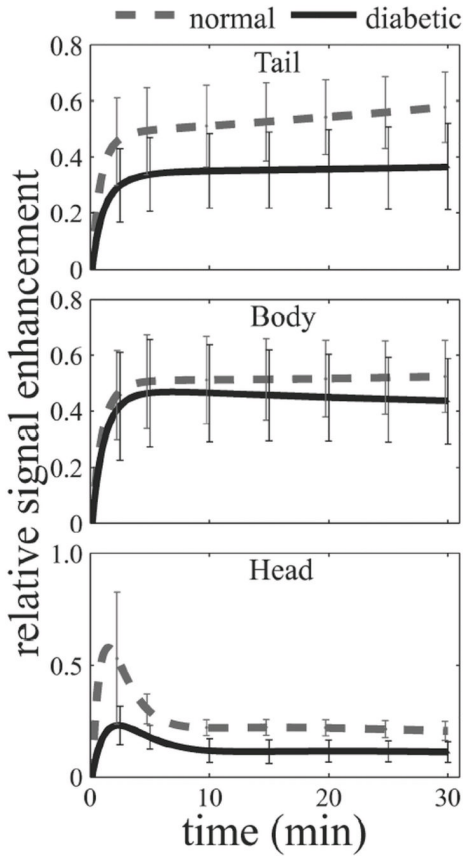

Figure 3.

Regional passive kinetic curves across the pancreas. Curves were generated using mean EMM parameters listed in Table 3. Error bars represent 2s. The rate of uptake in the normal tail was significantly greater than the diabetic. A comparison of the remaining kinetic parameters suggest a slower washout rate and a higher peak enhancement but without statistical significance ($p > 0.05$).

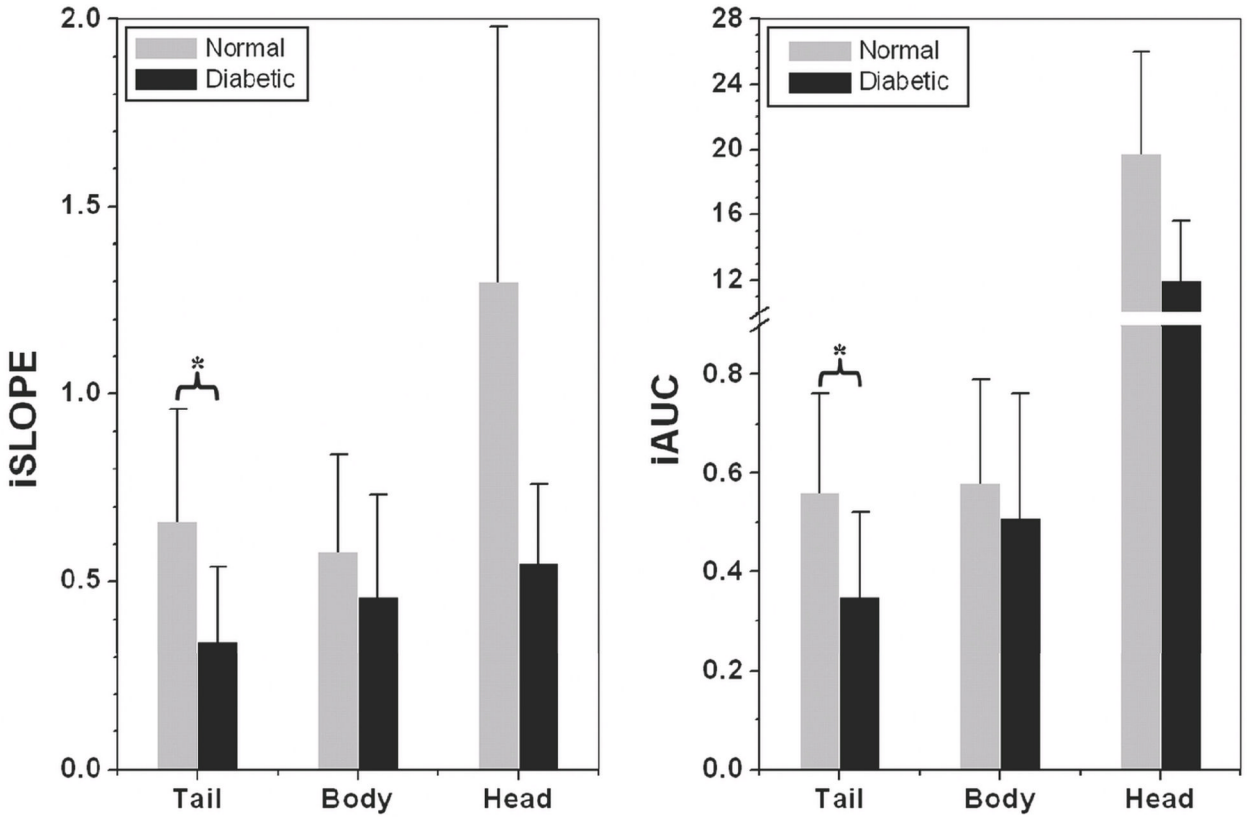

Figure 4.

Regional assessment of iSLOPE and iAUCτ in the normal and diabetic average secondary EMM parameters for the tail, body and head of the pancreas in normal and diabetic animals. (a) Initial slope (iSlope) and (b) Initial area under the curve at 2 min (iAUCτ) were found to be significantly steeper and larger in the normal pancreatic tail ($p < 0.05$) in comparison to the diabetic, but no significance was observed in the body and head. A '*' indicates statistical significance with a $p < 0.05$. **note: pancreatic head ROI data contained a blood vessel.

Table 1

Primary EMM parameters and angle between passive and active uptake curves for normal and diabetic mice kidneys. Parameters were averaged for the right and left kidney. The peak signal (A), uptake rate (α), and washout rate (β) derived from the EMM and the angle (θ) calculated from the linear function were not significantly different between normal and diabetic mice kidneys ($p > 0.2$ for EMM parameters and $p > 0.07$ for linear function parameters). Reported values are mean ± standard deviation.

	A	α (min^{-1})	β(min^{-1})	θ (degrees)
Normal Kidney	0.89±0.12	1.6±0.61	−0.004±0.005	0.45±0.39
Diabetic Kidney	0.86±0.11	1.4±0.42	−0.005±0.004	0.74±0.28

Table 2

Variation in Region of Interest (ROI) across animals and image slices. For each mouse, ROIs were identified based on reference images from all eight slices of the pancreas tail, body, and head and for the right and left kidneys. The average number of slices for each type of ROI was also calculated.

	Tail	Body	Head	Right Kidney	Left Kidney
Normal					
Number of mice with visible ROIs	11	9	7	11	8
Average number of ROI slices per mouse*	5	4	2	2	2
Diabetic					
Number of mice with visible ROIs	9	8	9	9	7
Average number of ROI slices per mouse*	6	4	3	3	3

*Average values were calculated over number of mice with visible ROIs, not total mice.

Table 3

Primary EMM parameters of passive uptake and change due to activation in normal and diabetic mouse pancreata. The peak signal (*A*), uptake rate (α), and washout rate (β) derived from the EMM and the angle (θ) calculated from the linear function were not significantly different between normal and diabetic mice pancreatic body and head. Uptake rate and angle were significantly greater in the pancreatic tail of normal mice ($p > 0.05$). Reported values are mean ± standard deviation.

	A	α (min^{-1})	β (min^{-1})	ε	γ (min^{-1})	θ (degrees)
Normal Pancreas						
Tail (n=11)	0.46±0.54	**1.4±0.54**	−0.008±0.007	-	-	**0.50±0.20**
Body (n=9)	0.50±0.17	1.2±0.34	−0.002±0.009	-	-	0.37±0.14
Head * (n=5)	0.57±0.09	0.2±0.16	0.011±0.010	19.75±16.70	0.64±0.17	0.33±0.31
Diabetic Pancreas						
Tail (n=9)	0.35±0.13	**1.0±0.44**	−0.001±0.01	-	-	**0.28±0.12**
Body (n=8)	0.48±0.21	0.90±0.38	0.003±0.009	-	-	0.40±0.30
Head * (n=5)	0.55±0.15	0.10±0.13	0.022±0.009	21.02±14.80	0.49±0.12	0.38±0.36

* Pancreatic head data with visible blood vessel.